Journal of Catalysis 266 (2009) 50–58

Contents lists available at ScienceDirect

Journal of Catalysis

journal homepage: www.elsevier.com/locate/jcat

CO oxidation by Ti- and Al-doped ZnO: Oxygen activation by adsorption on the dopant

Raj Ganesh S. Pala [a,1], Wei Tang [a,1], Michael M. Sushchikh [b], Jung-Nam Park [b], Arnold J. Forman [a], Guang Wu [a], Alan Kleiman-Shwarsctein [c], Jingping Zhang [c], Eric W. McFarland [b], Horia Metiu [a,*]

[a] Department of Chemistry and Biochemistry, University of California, Santa Barbara, CA 93106, USA
[b] Department of Chemical Engineering, University of California, Santa Barbara, CA 93106, USA
[c] Materials Department, University of California, Santa Barbara, CA 93106, USA

ARTICLE INFO

Article history:
Received 3 February 2009
Revised 20 April 2009
Accepted 13 May 2009
Available online 13 June 2009

Keywords:
CO oxidation
Catalysis
Doped oxide
Ti
Al
ZnO
$^{18}O_2$

ABSTRACT

Using a combination of theory and experiments, we show that ZnO substitutionally doped with Ti or Al oxidizes CO by several parallel reaction pathways that differ from the traditional Mars–van Krevelen (MVK) mechanism. In one, the dopant atoms at the surface of the doped oxide adsorb and activate O_2 so that it reacts with CO. In the other, a surface oxygen atom from the lattice next to the dopant, D, moves onto the dopant and creates an O-D group and an oxygen vacancy. The O-D group is capable of oxidizing a reductant. To test these predictions made by theory, we have prepared Ti- and Al-doped ZnO and have shown that these compounds oxidize CO at temperatures at which pure-phase ZnO, Al_2O_3, or TiO_2 do not. The proposed mechanisms were made plausible by studying CO oxidation with $^{18}O_2$.

1. Introduction

Oxide catalysts are widely used in industry [1–3] and much work is directed toward improving their performance and reducing the energy required for their use. One possible method for achieving these goals is to substitutionally exchange a small fraction of the cations at the host oxide surface [4–46]. We call the resulting compound a 'doped oxide' and the guest cation a 'dopant'. Given the large number of possible dopant-oxide pairs, it is hoped that some useful catalysts may be found in this class of compounds. Experimental progress in creating doped oxide catalysts has been slow, since there has been no systematic method for selecting dopant-host combinations and there are no sure-fire synthetic methods for placing substitutional dopants at the surface of the oxide. Moreover, if the doping level is low (e.g. ~1% of cations are substituted), it is difficult to rule out that the sample consists of a mixture of two oxides; or that it consists of extremely small (molecule sized) clusters of the dopant oxide on the surface of the host support; or that all dopant atoms are in the bulk of the sample. Quantum mechanical calculations have the advantage that they can unambiguously "prepare" and study substitutionally doped oxides. On the other hand, the calculations are performed on oxide slabs that may not be representative of the high-surface-area catalysts used in practice, and the real catalyst may have hydroxyls or even traces of carbonate on its surfaces caused by the presence of CO_2. In addition, it is suspected that density-functional theory has difficulties in describing accurately some of the oxides of interest to catalysis [47,48]. For these reasons, we use theory to qualitatively explore various possibilities and to predict the best candidates, then use experiments to test whether the suggestions made by theory can be translated into real-world catalysts.

Most heterogeneous oxidation reactions catalyzed by oxides take place via the Mars and van Krevelen (MVK) mechanism, in which the reductant (CO in our case) reacts with the oxygen atoms from the surface of the oxide [2,3,49]. The oxidized molecules desorb and take oxygen with them, leaving behind oxygen vacancies on the surface. These vacancies are filled by molecular oxygen from the gas phase, a step that completes the catalytic cycle. In previous computational studies, we have explored how doping the surface of TiO_2, CeO_2, and ZnO changes their oxidative power [50–52]. In the case of TiO_2 and CeO_2 all the dopants that we studied decrease the energy needed for forming oxygen vacancies and, therefore, make the oxide a better MVK oxidant. The increased oxidation activity was illustrated by a study of the catalytic cycle for CO oxidation [51,52].

* Corresponding author. Fax: +1 805 893 4120.
E-mail address: metiu@chem.ucsb.edu (H. Metiu).
[1] Contributed equally to the work.

0021-9517/$ - see front matter © 2009 Elsevier Inc. All rights reserved.
doi:10.1016/j.jcat.2009.05.011

In the case of ZnO, many dopants *increase* the energy that is necessary for removing an oxygen atom from the surface [50]; doping the oxide with them will *hinder* the oxidation through the MVK pathway. One would think that such doped oxides are less effective oxidation catalysts than the undoped host. In the present work, we consider two other possibilities that have been overlooked so far. The fact that the oxygen atoms near the dopant bind more strongly to the oxide indicates that the dopant is undercoordinated. This would imply that such a dopant will adsorb oxygen from the gas phase to satisfy its need for a higher coordination. If the dopant's valence is satisfied by binding one oxygen atom of gas-phase O_2, then the other O atom would be available for oxidizing a molecule. The net result is that the dopant adsorbs and activates O_2 from the gas phase, promoting oxidation reactions. Another possibility is that the undercoordinated dopant will "steal" an oxygen atom from the surface of the host oxide. This atom will settle on top of the dopant, leaving behind an oxygen vacancy in the surface layer. The oxygen on top of the dopant may be an active center for oxidation.

In this article, we present results of calculations and experiments that explore these two possibilities. To prove that CO is oxidized by O_2 adsorbed from the gas phase, we have performed the oxidation reaction with gas-phase $^{18}O_2$. We found that the catalyst produces $^{18}O^{16}O$, which proves that the oxygen atom that oxidizes CO originates from the gas-phase oxygen molecule. However, the reaction also produces comparable amounts of $C^{16}O_2$, and small amounts of $C^{18}O_2$. The formation of three CO_2 isotopes indicates that several distinct reaction mechanisms are at work in this system.

We have used sol–gel synthesis to attempt the preparation of high-surface-area ZnO atomically doped with Al or Ti. We have chosen to work with Ti, Al and Zn because TiO_2, Al_2O_3, or ZnO does not oxidize CO at temperatures below 450 °C, where we perform our experiments. Therefore, if the compound we prepare is active for CO oxidation at low temperatures, it cannot consist of separate bulk oxide phases. Since we use very small amounts of dopant precursor, it is likely that during synthesis the dopant atoms will not find each other to segregate and make a multiphase system consisting of ZnO and TiO_2 or Al_2O_3. Unfortunately, this argument does not rule out the possibility that we have prepared molecule-sized clusters of AlO_x or TiO_x supported on the surface of ZnO. In many cases, such supported molecule-sized oxide clusters are more active than the corresponding oxide [53,54] and may be responsible for the oxidation of CO.

2. Theoretical methodology

Since this is a combined theoretical and experimental study, we employ the following "division of labor". We use theory to identify energetically favored reaction pathways. We calculate the activation energy only for the most important steps: the reaction of CO with the adsorbed O_2 molecule and the formation of an oxygen vacancy by transfer of an oxygen atom from the surface onto the dopant. Since the calculations of activation energies are very time consuming and the values obtained are not very reliable, we preferred using experiments to test whether the doped oxides will convert CO to CO_2.

We use the density-functional theory implemented in the VASP code [55,56]. The electron-ion interaction is treated with the projector augmented wave method in which all the electrons except the valence ones are kept frozen [57]. The exchange-correlation energy is calculated with the PW-91 GGA functional [58]. The computed bulk lattice constants of ZnO were found to be $a = 3.282$ Å, $c/a = 1.6176$ and $u = 0.378$. The calculated heat of formation of ZnO is -3.41 eV, which is close to that observed in experiments [59,60] and in other computations [61–63]. A (2×3)-ZnO$(10\bar{1}0)$ surface super-cell with five layers was used in all calculations. Tests performed with a (3×4) super-cell show that an increase in slab thickness and super-cell size changes the adsorption energies by less than 0.05 eV. A plane-wave cut-off of 400 eV and a $2 \times 2 \times 1$ k-points grid was used for all calculations. For a few systems, we increased the k-points grid to $4 \times 4 \times 1$ and this changed the relative adsorption energies by less than 0.05 eV. The total energy is converged to within 10^{-3} eV/super-cell. We have allowed fractional occupancy of bands by using Gaussian smearing with an energy window of 0.05 eV. All calculations reported here take into account spin polarization.

Because DFT does not allow for rigorous description of spin of the many-body electronic wave function we enforce the conservation of spin polarization along the reaction path, as discussed in Refs. [64,65]. We do this because the internal magnetic fields felt by the electrons during the reaction are very weak, and the probability that the spin of an electron is changed during the reaction is very low. In this article we examine only the states allowed by spin conservation and if several spin states are allowed we report the evolution of the one having the lowest energy.

Density-functional theory seems to have some difficulties when applied to narrow band oxides [47,48]. It is not clear whether these difficulties result in errors in total energy differences, which are of interest to chemists; nor is it clear for which oxides or for which chemical processes the calculations are unreliable (it is conceivable that processes that do not involve changes in the population or the energy of the narrow bands are not affected). Because of this we focus on qualitative results and trends and, whenever possible, use experiments to settle more quantitative questions.

3. Oxygen activation by the dopant

In previous calculations [50], we have found that doping ZnO with Ti, V, Zr, Nb, Hf, Ta, or W increases substantially the energy required for making an oxygen vacancy at the surface of the oxide; Al, Mg, Ca, La, Re, Os and Ce have a similar, but less pronounced, effect. This indicates that these dopants are not satisfied with the number of oxygen atoms surrounding them and compensate by binding the neighboring oxygen more strongly. This is more pronounced for dopants whose preferred valence is higher than 2. It is likely that these "dissatisfied" dopants will tend to adsorb O_2 from the gas phase. If their valence is satisfied by binding to one additional O atom then the system will be inclined, after adsorbing an O_2 molecule, to provide the other oxygen atom for an oxidation reaction. Thus, ZnO doped with one of the dopants listed above is likely to adsorb O_2 and enhance its ability to engage in oxidation reactions. This mechanism is different from the usual Mars–van Krevelen (MVK) mechanism [49], which is invoked for explaining the majority of oxidation reactions catalyzed by oxides [66]. In MVK reactions, the reductant takes oxygen atoms out of the oxide surface, not from the gas phase. The role of O_2 in the gas phase is to prevent the complete reduction of the oxide by refilling the vacancies.

This qualitative argument prompted us to examine this idea in detail by studying the oxidation of CO by ZnO doped with Ti or Al. Our calculations found that O_2 adsorbs readily on the dopant and after that it reacts with CO. The subsequent evolution of the system is complicated: we found three possibilities, which are discussed below and illustrated by Figs. 1–3. All three mechanisms start with O_2 adsorption on the dopant (see structure Fig. 1b). This is highly exothermic for both Ti and Al. The O–O distance in the adsorbed oxygen molecule is ~1.53 Å, which is larger than the value of ~1.24 Å found by DFT for the gas-phase molecule. This increase in the bond length is a sign that the anti-bonding orbitals of O_2 are involved in the formation of the bond with the dopant. The

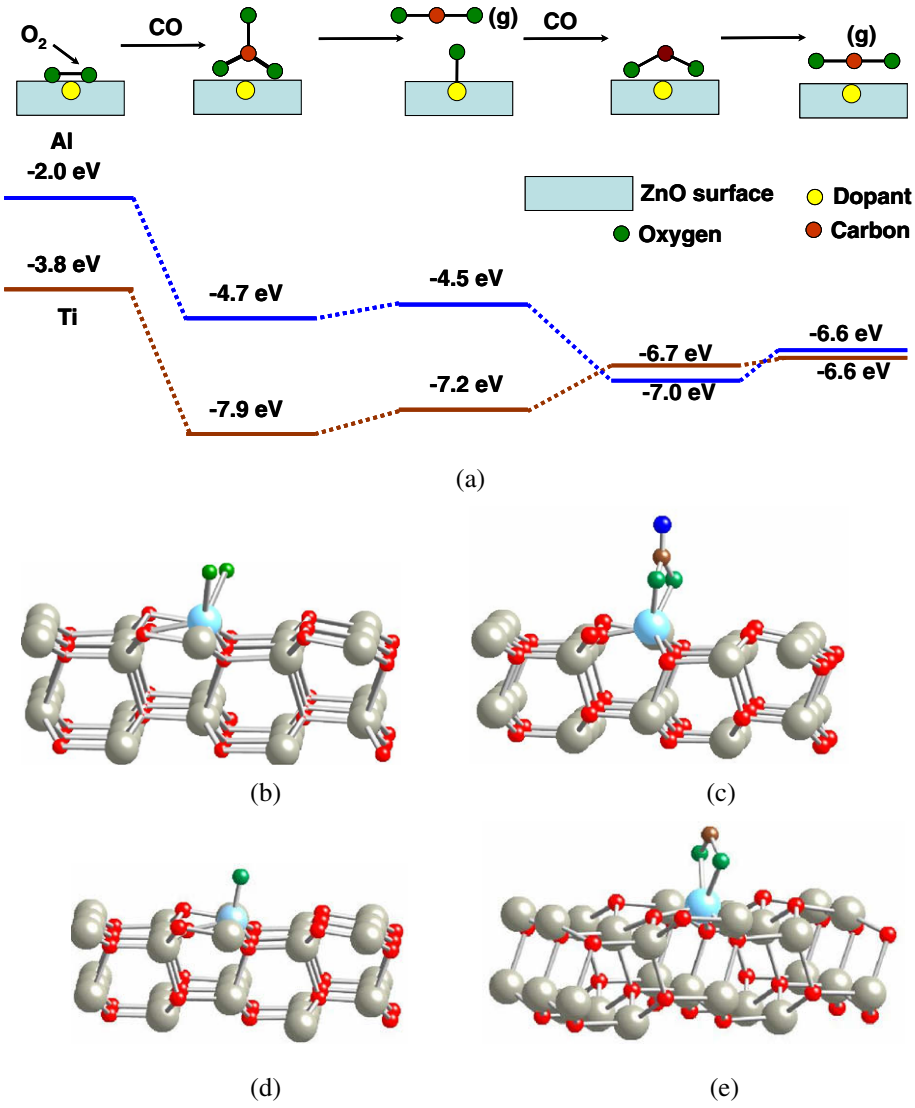

Fig. 1. The top row shows a schematic representation of the steps involved in Mechanism 1. The slab represents the ZnO, the yellow circle represents the dopant, the oxygen atoms coming from the gas phase are indicated in green, and the carbon atom is indicated in red. The (g) notation indicates that the molecule is in the gas phase. The second row shows the energy-level diagrams for the oxidation of two CO molecules with one O_2 molecule. The zero energy is that of the doped slab, and an O_2 molecule and two CO molecules in the gas phase. The last two rows show a stick and ball model of the pictures shown schematically in the first row. The pictures represent the structures that minimize the energy. The color of the spheres is coded as follows: oxygen atoms are indicated by red spheres, the Zn ones are indicated by gray spheres, the dopant is indicated in blue, the O atoms originating from the gas phase are indicated in green and the carbon atom is indicated in brown. (For interpretation of the references in color in this figure legend, the reader is referred to the web version of this article.)

Bader charge [67,68] on each adsorbed oxygen atom is ~−0.46, which supports the suggestion that the antibonding orbital in O_2 is populated when the molecule is adsorbed. The next step in all three mechanisms is the reaction of CO with the adsorbed oxygen to form a "carbonate" (see structure Fig. 1c), which takes place without an energy barrier. After these steps several mechanisms are possible.

3.1. Mechanism 1

The carbonate (Fig. 1c) decomposes to produce CO_2 in the gas phase, and leaves behind an oxygen atom bound to the dopant (Fig. 1d). This reacts with a second CO to form an "adsorbed CO_2 species" (Fig. 1e). The latter desorbs to produce CO_2 in the gas phase. This completes the catalytic cycle. The energy-level diagram in Fig. 1 shows that for the Al-doped catalyst (blue curve)[2] most steps in this mechanism are strongly exothermic, while two are mildly endothermic by 0.2 eV and 0.4 eV. For the Ti-doped oxide, the decomposition of the carbonate is uphill by 0.7 eV, and the reaction of CO with the adsorbed oxygen atom is uphill by 0.5 eV. These values are still small enough to make this mechanism plausible.

3.2. Mechanism 2

The second mechanism is illustrated by Fig. 2. The first two steps are the same as in Mechanism 1: O_2 adsorbs at the dopant site, reacts with CO to form a carbonate, which decomposes to produce CO_2 in the gas phase leaving an oxygen atom adsorbed on the dopant (we denote this by D-O). The distinction from Mechanism 1 starts in the next step: the Ti–O group adsorbs another oxygen molecule to form a "TiO_3" complex (see Fig. 2b). This reaction is exothermic for the Al-doped oxide and is endothermic by 0.4 eV for the Ti-doped one. The TiO_3 complex reacts with CO to form CO_2 in gas phase and O_2 adsorbed on the dopant,

[2] For interpretation of color in Fig. 1, the reader is referred to the web version of this article.

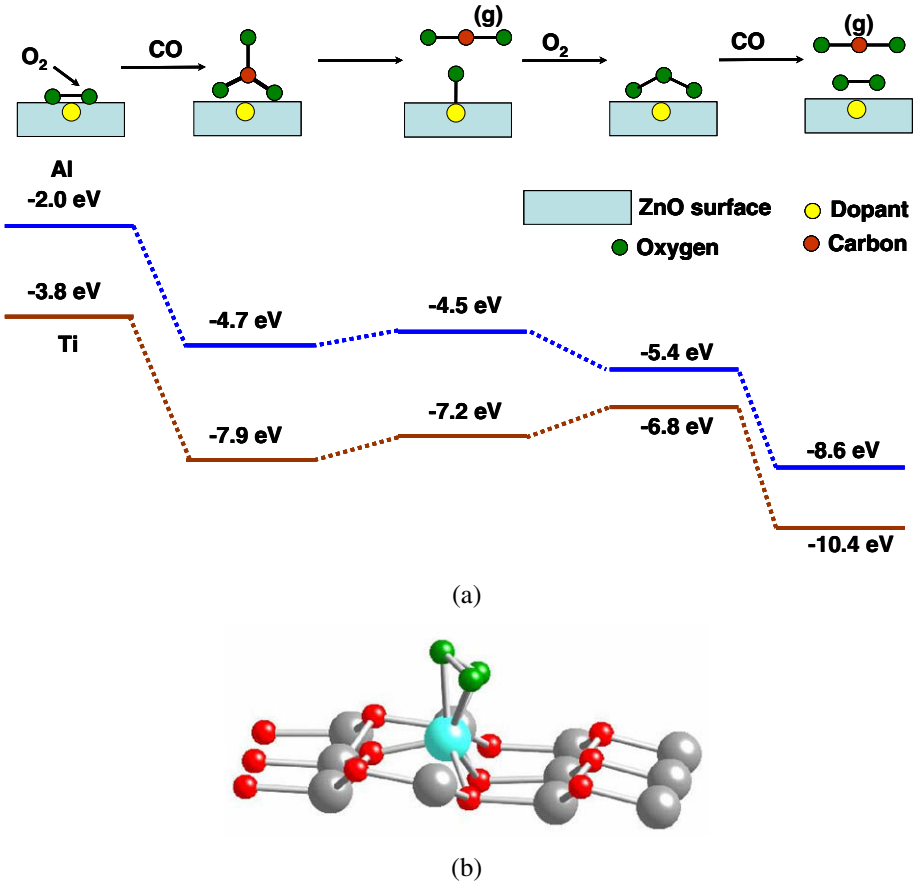

Fig. 2. A schematic representation of Mechanism 2. The caption is the same as that of Fig. 1 except that only the structure of the three oxygen atoms bound to the dopant (in (b)) is shown.

which closes the catalytic cycle. This reaction is strongly exothermic for both the dopants. All other things being equal, one would expect that mechanism 1 is favored when the CO pressure is higher than the O_2 pressure, since in this case the reaction of CO with Ti–O is more likely than the reaction of Ti–O with oxygen.

3.3. Mechanism 3

A third possible pathway is illustrated in Fig. 3, which also starts with oxygen adsorption followed by reaction with CO to form a carbonate. The carbonate can then react with another CO to form an oxalate whose structure is shown in Fig. 3b. The oxalate decomposes to form CO_2 and leaves an oxygen molecule on the dopant. Both reactions are exothermic.

We have calculated the binding energies of the compounds involved in these mechanisms to make sure that none contains reactions that are strongly "uphill". The activation energy was calculated only for one critical step: the reaction of the adsorbed O_2 with CO.

4. Experimental methodology

4.1. Catalyst synthesis

The $M_xZn_{1-x}O_\delta$ (M = Al, Ti) powder catalysts were synthesized from sol–gel precursors. Solutions were prepared by mixing 1% (metals basis) of the dopant butoxide (aluminum butoxide or titanium (IV) butoxide (Sigma–Aldrich)) with $Zn(NO_3)_2{\cdot}6H_2O$ (Fisher) in isopropanol (EMD). The solution was stirred for approximately 30 min, until the precursors were dissolved, and then capped and stirred for an additional 30 min to insure adequate mixing. The solution was then uncapped and placed into a water bath at 70 °C to evaporate the solvent and simultaneously hydrolyze the precursors using water from moisture in the ambient air and in the precursor solutions. The solution gels and appears white after approximately two hours. The gel was pre-dried in a water bath at 100 °C for 2 h, then calcined in air at 1000 °C for 6 h. The ZnO control material was prepared identically except no dopant metal butoxide was added.

4.2. Catalyst characterization

The morphology of the powder sample was characterized by scanning electron microscopy (SEM, FEI XL40 Sirion FEG Digital Scanning Microscope) and transmission electron microscopy (TEM, FEI Titan FEG High Resolution TEM/STEM operated at 300 kV). The detailed elemental distribution was obtained from energy dispersive X-ray spectroscopy (EDS) using the instrument attached to the TEM, (FEI Titan 300 kV FEG TEM/STEM System w/EDS & EELS). The surface area was determined by BET analysis (Tristar 3000 Gas Absorption Analyzer, Micromeritics). The powder X-Ray Diffraction (XRD) spectra were measured with a Scintag X2 diffractometer, with a 2 kW Cu anode and a solid-state point detector. The XRD data were processed using the Windows version of the Scintag data collection and analysis package. The Rietveld refinement of the XRD data was simulated using a General Structure Analysis System (GSAS) to obtain the fractional dopant concentrations from the changes in the lattice spacing.

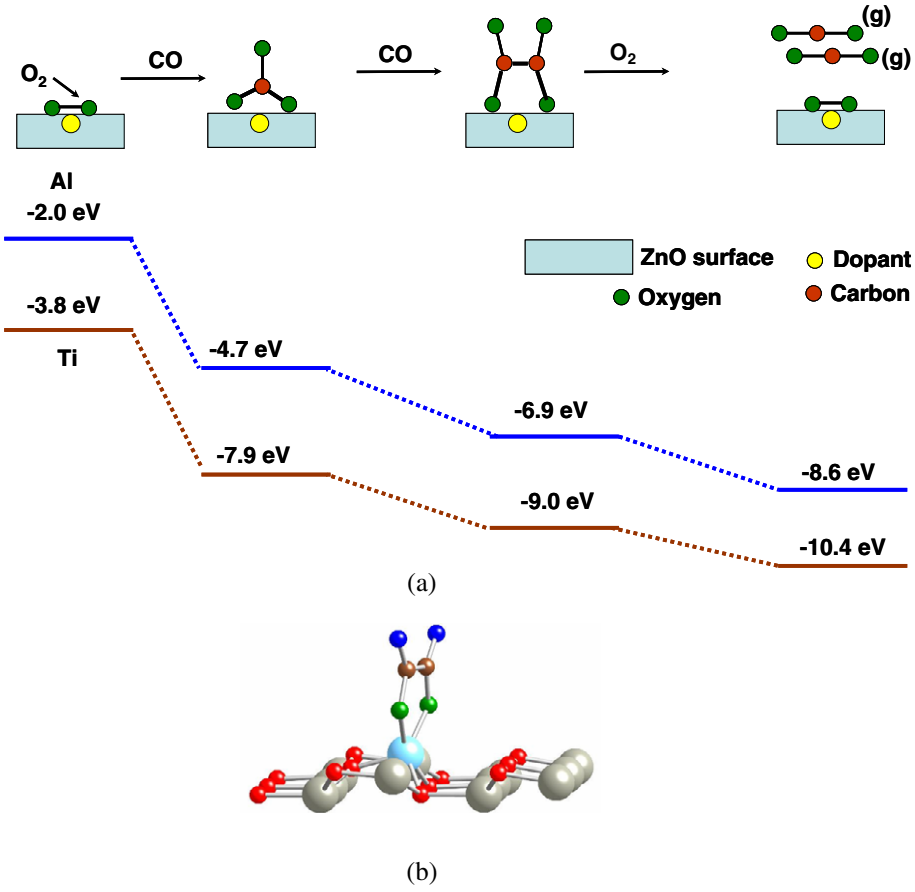

Fig. 3. A schematic representation of Mechanism 3. The caption is the same as that of Fig. 1 except that only the structure of the oxalate bound to the dopant (in (b)) is shown.

4.3. Catalyst testing

The activity of the metal oxide catalyst was measured in a packed bed reactor (PBR) using argon as a carrier gas and calibration standard. The PBR was a 6 mm diameter glass tube, 300 mm in length, which was fitted inside an aluminum heating block. In a typical run approximately 250 mg of catalyst was used in an active reaction volume of 0.25 ml. The void fraction was approximately 82%. The volumetric flow rates of argon, carbon monoxide and oxygen were controlled by mass flow controllers (MKS). Typical experimental flow rates were 3.7 ml/min for argon, 9.7 ml/min for oxygen and 9.7 ml/min for carbon monoxide, with an approximate space time of 0.3 s. The product gas was sampled directly at the reactor outlet into a differentially pumped mass spectrometer (SRS) through a controlled leak valve.

For temperature-programmed reaction (TPR) studies, the temperature was ramped at a rate of 7.5 K/min using a programable controller (Omega, CSC32). For Fourier transform infrared (FTIR) (Thermo Electron Corporation, Nicolet 4700) studies, the catalysts were exposed to the same flow rate of gases at temperatures up to 400 °C with automated temperature control (Harrick). Partial pressure-programmed reaction experiments were conducted at a constant temperature of (450 °C) and a constant total flow rate of 23 ml/min. The flow rates of carbon monoxide, oxygen and argon were varied to change the CO/O_2 ratio while maintaining a constant total flow rate.

The reaction with isotopically labeled oxygen, $^{18}O_2$ (ISOTEC), was performed by pre-treating the catalyst to remove all absorbed $^{16}O_2$: the catalyst was heated to 375 °C in an Ar flow rate of 3.7 ml/min for 1 h, followed by 1 h of exposure to CO at a flow rate of 9.7 ml/min at 375 °C, and then another hour in Ar at 375 °C. While flowing CO and Ar at flow rates of 9.7 ml/min and 3.7 ml/min respectively, the $^{18}O_2$ was introduced in pulses (3–5 s) using a two-position microelectric valve (VICI).

5. Experimental results

5.1. Physical characterization of doped ZnO

SEM images show that after calcination at 1000 °C, ZnO forms micron-sized crystallites (Fig. 4a). Al- and Ti doping leads to the creation of more edge and corner sites (Fig. 4b and c). The Ti-doped ZnO showed an insignificant BET surface area increase, after calcination, from 0.24 m^2/g to 0.25 m^2/g; however, the surface area of the Al-doped ZnO increased to 0.39 m^2/g.

High-resolution transmission electron microscopy (HRTEM) with line-scan EDS was also used on approximately 10 different areas for each sample. Bright field, high angle annular dark field (HAADF) scanning TEM (STEM) images with sub-nanometer resolution combined with selected area line-scan EDS showed the Al-doped ZnO to be uniform. For the Ti-doped ZnO, a small amount of Ti enrichment was observed by line-scan EDS at the surface of the ZnO crystallites. These two EDS experiments suggest that ZnO is doped uniformly without creation of regions of high dopant concentration.

Qualitatively, all XRD spectra indicate a singular phase matching: those of pure ZnO. Rietveld refinement of the XRD data for Al-doped ZnO, Fig. 5, shows that the lattice contracts from 3.2507 Å to 3.2499 Å along the a- and b-axis, and expands from 5.2051 Å to 5.2066 Å along the c-axis vs. pure ZnO. The refinement indicates that Al was doped into the ZnO lattice at an atomic fraction of 0.99%. This is in agreement with the 1% mole ratio of Al in

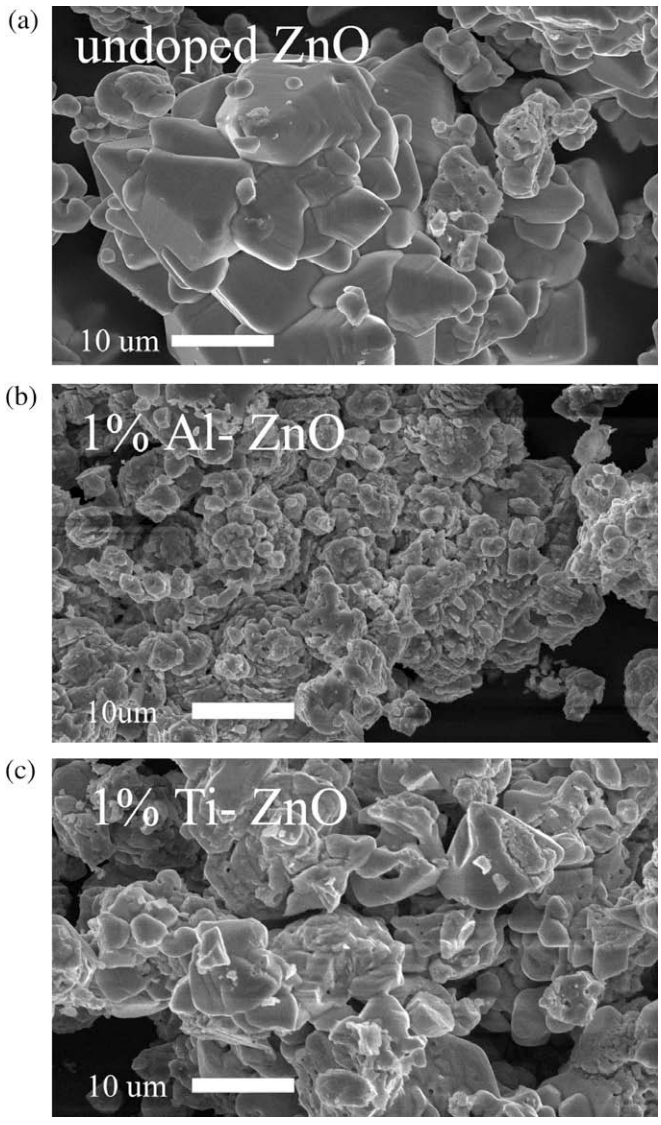

Fig. 4. Scanning electron micrographs of (a) ZnO and ZnO doped with (b) Al or (c) Ti.

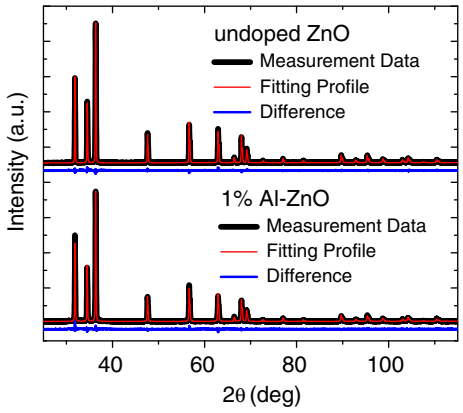

Fig. 5. XRD spectra (black line) of ZnO and ZnO doped with 1% Al. The XRD data fit by using the Rietveld refinement is shown in red. The difference between the data and the calculation based on the Rietveld refinement is shown in blue. (For interpretation of the references in color in this figure legend, the reader is referred to the web version of this article.)

Zn used in the synthesis. No significant lattice change was observed by Rietveld refinement of the Ti-doped ZnO, which is likely due to a similar size of the Ti and Zn cations. The XRD and Rietveld studies suggest that the materials are of a uniform phase and do not consist of a phase of the dopant's oxide and one of the host oxide.

5.2. CO oxidation by $^{16}O_2$

Fig. 6a shows the TPR results for oxidation of carbon monoxide on doped and undoped ZnO. The low-temperature activity (300–

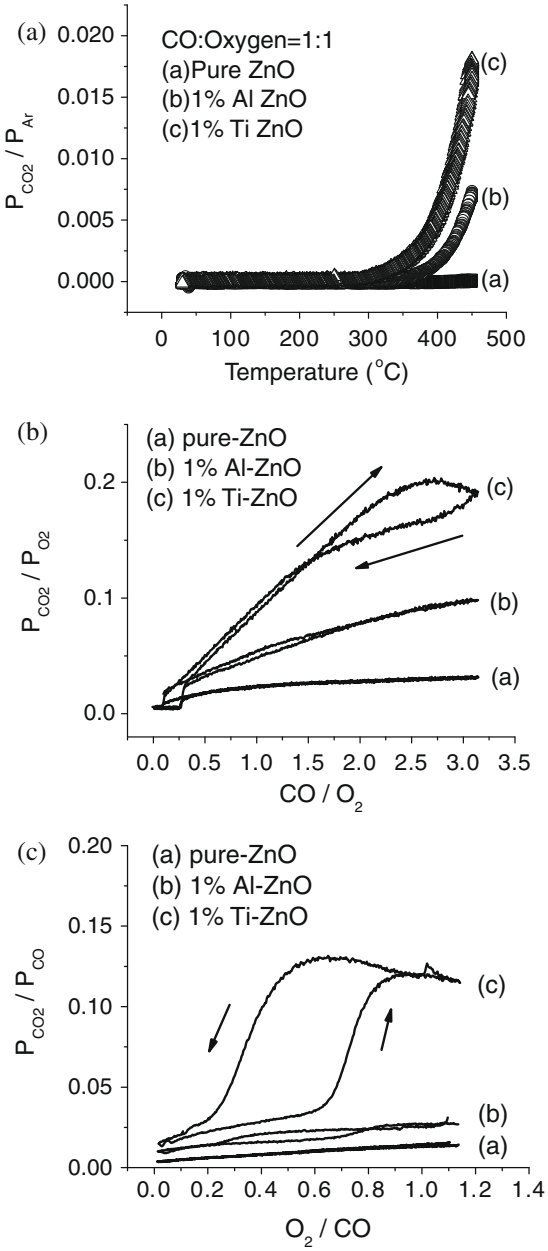

Fig. 6. CO oxidation by $^{16}O_2$ (a) temperature-programmed reaction for ZnO and ZnO doped with Ti or Al; products monitored by mass spectroscopy. The measured partial pressure of CO_2 was normalized to the partial pressure of the Ar carrier gas. (b) Partial pressure-programmed reaction of ZnO and ZnO doped with Ti or Al; O_2 partial pressure is held constant while CO partial pressure is varied; a constant flow rate and reaction times are maintained by adjusting the flow rate of Ar. The measured partial pressure of CO_2 was normalized to the partial pressure of oxygen. (c) Partial pressure-programmed reaction of ZnO and ZnO doped with Ti or Al; CO partial pressure is held constant while the O_2 partial pressure is varied. By changing the flow rate of Ar, we maintain a constant total flow rate and reaction space time. The measured partial pressure of CO_2 was normalized to the partial pressure of CO.

400 °C) for the Ti- and Al-doped ZnO was significantly greater than that for the undoped ZnO control sample, which has extremely low activity in this temperature range. The Ti-doped samples were more active than those doped with Al, which could be due to a greater density of active sites on the Ti-enriched surface as observed in HRTEM EDS measurements. With in situ FTIR, under the same reaction conditions at 400 °C, absorption peaks were observed at 1560 cm^{-1} and 1370 cm^{-1}, which are attributed to –OCO– and C=O stretches in the Ti–O_2CO complex [69]. The observation of these bidentate peaks is consistent with the mechanism proposed in Fig. 1. No bidentate peaks were observed for the Al-doped sample under identical conditions.

Fig. 6b shows the change in the activity, at 450 °C, when the partial pressure of CO is varied and that of O_2 is held constant. Fig. 6c shows the change in the activity, when the partial pressure of O_2 is varied and that of CO is held constant. In both the cases, a hysteresis is observed for Ti-doped ZnO and a reversible behavior is observed for Al-doped ZnO.

5.3. CO oxidation by $^{18}O_2$

The main point of this paper is that the mechanism of CO oxidation on Ti- or Al-doped ZnO differs from that of Mars–van Krevelen; the oxidation is due to the adsorbed oxygen molecule, not by the oxygen atoms at the surface of the oxide. To test this hypothesis, we have performed the reaction with gaseous $^{18}O_2$. If the oxidation is caused by the adsorbed oxygen, the reaction will produce $C^{18}O^{16}O$; if the mechanism is Mars–van Krevelen, the product will be $C^{16}O_2$. Fig. 7a shows the partial pressure of CO, Ar and O_2 in the mass spectrometer, at the exit from the reactor, for Ti-doped ZnO. We introduce CO and Ar continuously, without oxygen, and then use a 5 s oxygen pulse, followed by a 3 min oxygen pulse. The reaction is run at 350 °C. The total pressure in the mass spectrometer is held constant and pulsing O_2 lowers the partial pressure of CO and Ar. In addition, the partial pressure of CO is diminished by its oxidation. Fig. 7b shows the partial pressure of the isotopes of CO_2 produced under the conditions used in Fig. 7a. We have measured the amount of $C^{16}O_2$ impurity in CO and have removed this contribution from the $C^{16}O_2$ produced by the reaction. If all CO were oxidized exclusively by the gas-phase $^{18}O_2$, we would have observed only $C^{16}O^{18}O$. The presence of $C^{16}O_2$ and $C^{18}O_2$ indicates that additional mechanisms are at work. Fig. 7c shows the 5 s oxygen pulse used to oxidize CO on undoped ZnO. Since the undoped oxide is considerably less active than the doped oxide, we use a temperature of 450 °C for this experiment. The partial pressure of various CO_2 isotopes, at the exit of the reactor, is shown in Fig. 7d. Note that the partial pressure scale is an order of magnitude smaller than that in Fig. 7b. The ratio of $C^{16}O_2$ to $C^{18}O^{16}O$ is much higher for the undoped oxide than for the doped one. We assume that the $C^{18}O^{16}O$ is produced after some ^{16}O atoms in the surface are exchanged with ^{18}O. The fact that the ratio of mass 44 to mass 46 changes from 8:1 (on pure ZnO) to 3:2 (in 1% Ti-doped ZnO) is evidence that the non-Mars–van Krevelen mechanism is dominant in the Ti-doped material. In all these

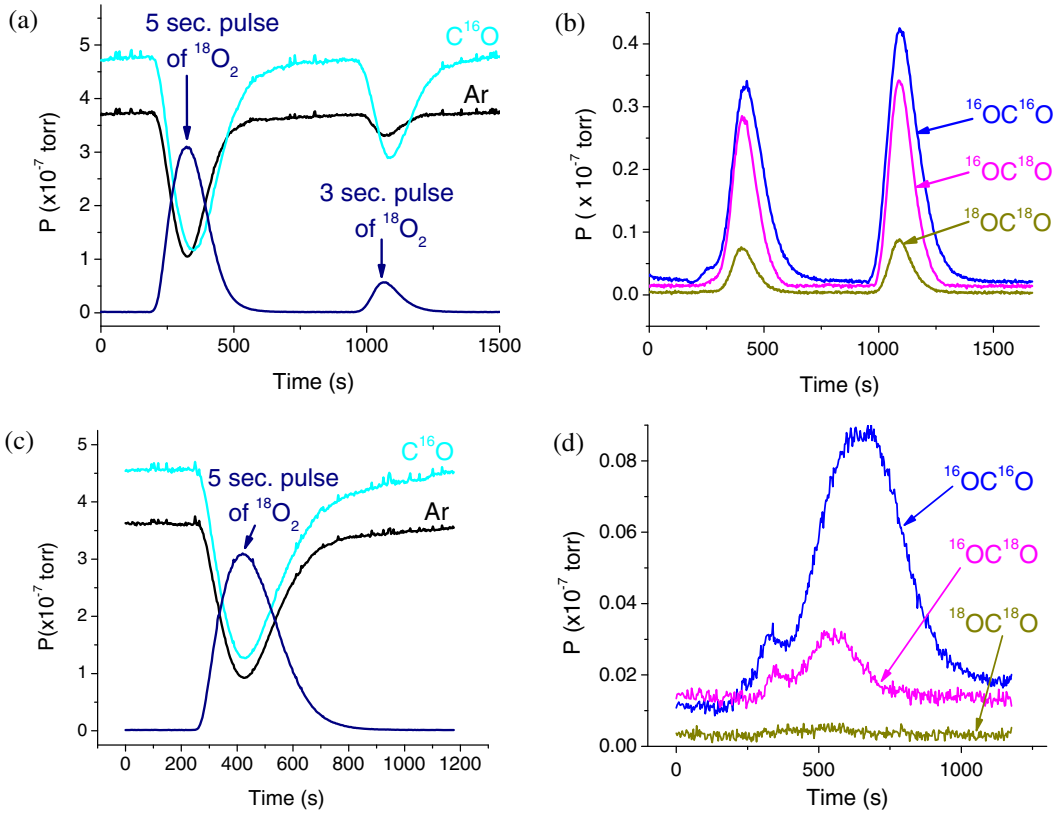

Fig. 7. (a) The partial pressure of CO, O_2, and Ar in the mass spectrometer at the exit of the reactor when O_2 pulses are introduced. The reaction, which is catalyzed by Ti-doped ZnO, takes place at 350 °C. The total pressure is constant and the introduction of the oxygen pulse lowers the partial pressure of Ar and CO. In addition, CO is consumed and the CO/Ar ratio is smaller than that obtained prior to the introduction of oxygen. The duration of the first pulse is 5 min, that of the second pulse is three minutes. (b) The partial pressure of various CO_2 isotopes produced by the pulses shown in (a), for the Ti doped ZnO catalyst, at 350 °C. Blue for $C^{16}O_2$, magenta for $C^{16}O^{18}O$, and dark green for $C^{18}O_2$. The second, shorter pulse, produces more CO_2 than the first one. This happens because the first pulse changes the state of the surface. (c) The partial pressures of O_2, CO and Ar when an O_2 pulse is introduced in the system. The temperature is 450 °C, the catalyst used is ZnO, and the pulse duration is 5 min. (d) The CO_2 isotopes produced by CO oxidation on ZnO at 450 °C, by the pulse described at (c). The temperature is higher than that in the case of Ti-doped ZnO, the scale is smaller and the ratio of $C^{18}O^{16}O$ to $C^{16}O_2$ is lower than that obtained in (c). (For interpretation of the references in color in this figure legend, the reader is referred to the web version of this article.)

experiments, care was taken to remove any $^{18}O_2$ adsorbed in the previous experiment.

The presence of $C^{18}O_2$ and $C^{16}O_2$, along with the expected $C^{18}O^{16}O$, surprised us. None of the three mechanisms proposed in Section 3 would produce them. We need to invoke additional mechanisms and we do this in the next section.

6. Additional mechanisms

The formation of $C^{16}O_2$ has to involve ^{16}O atoms from the surface of the oxide, which suggests a Mars–van Krevelen or a MVK-like mechanism. In our previous work, we had shown that in the case of Au-doped ceria [52] or Au-doped rutile titania [51], the presence of the dopant weakens the bond of a surface oxygen atom to the oxide, and that oxygen atom reacts with CO to make a CO_2 molecule. Our calculations show that this mechanism does not operate for the doped oxides studied here. This is not surprising since it was found [50] that doping with Al or Ti makes the oxygen atoms at the surface of ZnO bind more strongly to the oxide than in the case of the undoped surface. We found, however, that an oxygen atom from the surface layer can move on top of the dopant to create a ^{16}O–Ti group and an oxygen vacancy on the surface layer near the dopant. The activation energy for this process is 0.2 eV. The reaction path is shown in Fig. 8. We think that this is not peculiar to the $Ti_xZn_{1-x}O$ system. Calculations have shown [65] that if $V_xTi_{1-x}O_2$, $W_xTi_{1-x}O_2$, $Mo_xTi_{1-x}O_2$, or $Cr_xTi_{1-x}O_2$, with the dopant in the surface layer, are in contact with gaseous O_2, the compounds $(VO)_xTi_{1-x}O_2$, $(WO)_xTi_{1-x}O_2$, $(MoO)_xTi_{1-x}O_2$, or $(CrO)_xTi_{1-x}O_2$ in which an oxygen atom is bound on top of the dopant are more stable than the doped oxide and $1/2O_2$ in the gas phase. This is not a general feature, though Mn_xTiO_2 with $1/2O_2$ in the gas phase is more stable than $(MnO)_xTi_{1-x}O_2$.

The fact that an oxygen atom from the ZnO surface can climb on top of the Ti dopant (and create an oxygen vacancy in the surface) gives rise to Mechanism 4: the ^{16}O–Ti group reacts with $C^{16}O$ to form $C^{16}O_2$. This explains the presence of this species among our products. Each desorbed CO_2 creates an oxygen vacancy on the surface. To have a catalytic reaction, the surface must be re-oxidized. It is very likely that $^{18}O_2$ adsorbs at the vacancy site and will then react with CO to produce $C^{16}O^{18}O$, which desorbs and annihilates the vacancy. Another possibility is that $^{18}O_2$ adsorbs at the vacancy site and dissociates, filling the vacancy and producing an ^{18}O which later reacts with $C^{16}O$ or finds another vacancy. O_2 dissociation at vacancy sites has been observed in STM experiments [64,70–72] with reduced $TiO_2(110)$ and in DFT calculations, in which spin conservation has been imposed [64]. We have not performed calculations to explore these possibilities for $Ti_xZn_{1-x}O$. However, it is clear that no matter which of these alternatives take place, the result is that the surface will slowly accumulate ^{18}O at sites near the dopant atoms. Our experiments used a pulse of $^{18}O_2$ and, therefore, did not deplete the surface oxide significantly of ^{16}O.

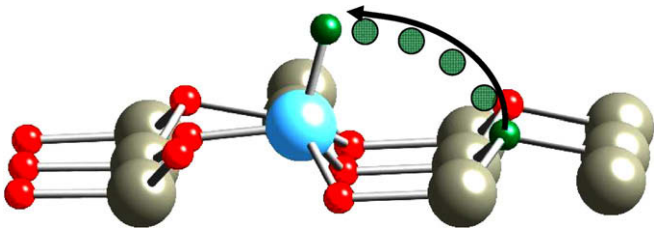

Fig. 8. Reaction pathway for an oxygen atom moving on top of the dopant from the first surface layer of the oxide. The oxygen atoms are indicated in red, zinc is indicated in gray, the dopant is indicated in blue, and the green sphere indicates the oxygen vacancy left behind when the O atoms move onto the dopant. The light green circles indicate the positions of the O atom along the reaction path (from oxide to the dopant). (For interpretation of the references in color in this figure legend, the reader is referred to the web version of this article.)

We note that the adsorption of O_2 on the dopant, required by Mechanisms 1–3, has no barrier and is strongly exothermic. The adsorption of O_2 on Ti competes with the formation of Ti–O, required by Mechanism 4, which has a barrier of 0.2 eV. Therefore, Mechanism 4 is expected to be less efficient than Mechanisms 1–3, especially at high partial pressures of O_2.

A plausible explanation is presented for the observed $C^{16}O_2$ even though the reaction does not go through a traditional Mars–van Krevelen mechanism (i.e., CO does not react directly with an oxygen atom from the surface layer, but reacts with an oxygen atom on top of the dopant).

We do not have a firm explanation for the appearance of $C^{18}O_2$. It is possible that when the carbonate or the oxalate is formed the oxygen atoms may rearrange and $C^{18}O_2$ is formed from the carbonate $C^{16}O^{18}O_2$ or from the oxalate.

7. Summary

We propose and demonstrate two CO oxidation pathways that are different from the traditional MVK mechanism. We have shown that cationic substitutional doping of ZnO with Ti or Al promotes adsorption of O_2 on the dopant. Essentially, this happens because Ti and Al have a higher valence than Zn. When these dopants replace a Zn atom, at the surface of ZnO, they do not find enough lattice oxygen atoms to satisfy their valence. This drives them to adsorb gas-phase O_2. Because these particular dopants would prefer to have one additional oxygen atom, rather than two, the adsorbed O_2 molecule reacts readily with a reductant. For CO, the oxidation can take place by three mechanisms that will produce $C^{18}O^{16}O$ if the gas-phase oxygen is $^{18}O_2$ and by a fourth mechanism that will produce $C^{16}O_2$. We have not performed the calculations necessary for sorting out which mechanism prevails under a given set of conditions. It is quite possible that all these take place simultaneously, with different reactions occurring at different dopant sites.

We believe that the fact that the dopant has a higher valence than Zn explains qualitatively the behavior of the doped oxide. There is, however, a second relevant factor: the Zn atoms do not adjust its valence to respond to the presence of a dopant; in the Zn–O–Ti groups present on the surface, Zn will stay divalent. CuO doped with Ti or Al would behave differently than ZnO in this respect, because in the group Cu–O–Ti, Cu may become monovalent to give the dopant a chance to bind more strongly to the shared oxygen atom. Therefore, we speculate that the mechanism presented here works better if the cations of the host oxide have only one stable oxidation state.

We have also found that an oxygen atom from the surface may migrate onto the dopant atom, and then react with CO. This mechanism explains the presence of $C^{16}O_2$ products when the gas-phase oxygen is $^{18}O_2$.

We speculate that numerous other oxides doped with cations having a higher valence than the host will behave like the present system in oxidation reactions, especially if the cation in the host is not able to reduce its valence when the dopant is present.

Acknowledgments

This work was supported by the Air Force Office of Scientific Research under Grant No. FAA9550-06-1-0167 and by the U.S. Department of Energy Division of Basic Energy Sciences (DE-FG03-89ER14048). We are grateful to the California Nanoscience Institute for providing computing time for our work.

References

[1] C.H. Bartholomew, R.J. Farrauto, Industrial Catalytic Processes, John Wiley & Sons, New York, 2006.
[2] B.K. Hodnett, Heterogeneous Catalytic Oxidation, John Wiley & Sons, New York, 2000.
[3] J. Haber, Oxygen in Catalysis, Marcel Dekker Inc., New York, 1991.
[4] A. Cimino, M. Sciavello, F.S. Stone, Discuss. Farad. Soc. 41 (1966) 350.
[5] A. Cimino, F.S. Stone, Adv. Catal. 47 (2002) 141.
[6] Y. Nishihata, J. Mizuki, T. Akao, H. Tanaka, M. Uenishi, M. Kimura, T. Okamoto, N. Hamada, Nature 418 (2002) 164.
[7] H. Tanaka, N. Mizuno, M. Misono, Appl. Catal. A 244 (2003) 371.
[8] H. Tanaka, I. Tan, M. Uenishi, M. Kimura, K. Dohmae, Topics Cat. 16/17 (2001) 63.
[9] H. Tanaka, I. Tan, M. Uenishi, M. Taniguchi, M. Kimura, Y. Nishihata, J. Mizuki, J. Alloy Compd. 408 (2006) 1071.
[10] H. Tanaka, M. Taniguchi, N. Kajita, M. Uenishi, I. Tan, N. Sato, K. Narita, M. Kimura, Top. Catal. 30/31 (2004) 389.
[11] H. Tanaka, M. Taniguchi, M. Uenishi, N. Kajita, I. Tan, Y. Nishihata, J. Mizuki, K. Narita, M. Kimura, K. Kaneko, Angew. Chem. Int. Ed. 45 (2006) 5998.
[12] H. Tanaka, M. Uenishi, M. Taniguchi, I. Tan, K. Narita, M. Kimura, K. Kaneko, Y. Nishihata, J. Mizuki, Catal. Today 117 (2006) 321.
[13] T. Baidya, A. Gayen, M.S. Hegde, N. Ravishankar, L. Dupont, J. Phys. Chem. B 110 (2006) 5262.
[14] T. Baidya, M.S. Hegde, J. Gopalakrishnan, J. Phys. Chem. B 111 (2007) 5149.
[15] T. Baidya, A. Marimuthu, M.S. Hegde, N. Ravishankar, G. Madras, J. Phys. Chem. C 111 (2007) 830.
[16] M.B. Bellakki, A.S. Prakash, C. Shivakumara, M.S. Hegde, A.K. Shukla, Bull. Mater. Sci. 29 (2006) 339.
[17] P. Bera, S.T. Aruna, K.C. Patil, M.S. Hegde, J. Catal. 186 (1999) 36.
[18] P. Bera, A. Gayen, M.S. Hegde, N.P. Lalla, L. Spadaro, F. Frusteri, F. Arena, J. Phys. Chem. B 107 (2003) 6122.
[19] P. Bera, M.S. Hegde, Catal. Lett. 79 (2002) 75.
[20] P. Bera, S. Malwadkarb, A. Gayena, C.V.V. Satyanarayanab, B.S. Raob, M.S. Hegde, Catal. Lett. 96 (2004) 213.
[21] P. Bera, K.R. Priolkar, A. Gayen, P.R. Sarode, M.S. Hegde, S. Emura, R. Kumashiro, V. Jayaram, G.N. Subbanna, Chem. Mater. 15 (2003) 2049.
[22] P. Bera, K.R. Priolkar, P.R. Sarode, M.S. Hegde, S. Emura, R. Kumashiro, N.P. Lalla, Chem. Mater. 14 (2002) 3591.
[23] G. Dutta, U.V. Waghmare, T. Baidya, M.S. Hegde, K.R. Priolkar, P.R. Sarode, Chem. Mater. 18 (2006) 3249.
[24] G. Dutta, U.V. Waghmare, T. Baidya, M.S. Hegde, K.R. Priolkar, P.R. Sarode, Catal. Lett. 108 (2006) 165.
[25] A. Gayen, T. Baidya, K. Biswas, S. Roy, M.S. Hegde, Appl. Catal. A 315 (2006) 135.
[26] A. Gayen, K.R. Priolkar, P.R. Sarode, V. Jayaram, M.S. Hegde, G.N. Subbanna, S. Emura, Chem. Mater. 16 (2004) 2317.
[27] A. Gayen, K.R. Priolkar, A.K. Shukla, N. Ravishankar, M.S. Hegde, Mater. Res. Bull. 40 (2005) 421.
[28] L. Pino, V. Recupero, S. Benianati, A.K. Shukla, M.S. Hegde, P. Bera, Appl. Catal. A 225 (2002) 63.
[29] S. Roy, M.S. Hegde, N. Ravishankar, G. Madras, J. Phys. Chem. C 111 (2007) 8153.
[30] S. Roy, A. Marimuthu, M.S. Hegde, G. Madras, Appl. Catal. B 73 (2007) 300.
[31] S. Roy, A. Marimuthu, M.S. Hegde, G. Madras, Appl. Catal. B 71 (2007) 23.
[32] S. Sharma, M.S. Hegde, Catal. Lett. 112 (2006) 69.
[33] F.J. Perez-Alonso, I. Melian-Cabrera, M. Loper Granados, F. Kapteijs, J.L.G. Fierro, J. Catal. 239 (2006) 340.
[34] M.F. Wilkes, P. Hayden, A.K. Bhattacharya, J. Catal. 219 (2003) 295.
[35] M. Zamora, T. Lopez, R. Gomez, M. Asomoza, R. Melendez, Catal. Today 107–108 (2005) 289.
[36] T. Ito, J.H. Lunsford, Nature 314 (1985) 721.
[37] T. Ito, J.X. Wang, C.H. Lin, J.H. Lunsford, J. Am. Chem. Soc. 107 (1985) 5062.
[38] C. Shi, M. Hatano, J.H. Lunsford, Catal. Today 13 (1992) 191.
[39] S. Fuchs, L. Leveles, K. Seshan, L. Lefferts, A. Lemidou, J.A. Lercher, Top. Catal. 15 (2001) 169.
[40] S. Gaab, J. Find, T.E. Muller, J.A. Lercher, Top. Catal. 46 (2007) 101.
[41] L. Leveles, S. Fuchs, K. Seshan, J.A. Lercher, L. Lefferts, Appl. Catal. A 227 (2002) 287.
[42] L. Leveles, K. Seshan, J.A. Lercher, L. Lefferts, J. Catal. 218 (2003) 307.
[43] L. Leveles, K. Seshan, J.A. Lercher, L. Lefferts, J. Catal. 218 (2003) 296.
[44] C. Trionfetti, I.V. Babich, K. Seshan, L. Lefferts, Appl. Catal. A 310 (2006) 105.
[45] T. Berger, J. Schuh, M. Sterrer, O. Diwald, E. Knozinger, J. Catal. 247 (2007) 61.
[46] N.A.S. Amin, S.E. Pheng, Chem. Eng. J. 116 (2006) 187.
[47] M.V. Ganduglia-Pirovano, A. Hoffmann, J. Sauer, Surf. Sci. Rep. 62 (2007) 219.
[48] G. Pacchioni, J. Chem. Phys. 128 (2008) 182505.
[49] P. Mars, D.W. van Krevelen, Chem. Eng. Sci. Spec. Suppl. 3 (1954) 41.
[50] R.G.S. Pala, H. Metiu, J. Phys. Chem. C 111 (2007) 8617.
[51] S. Chrétien, H. Metiu, Catal. Lett. 107 (2006) 143.
[52] V. Shapovalov, H. Metiu, J. Catal. 245 (2007) 205.
[53] I.E. Wachs, Catal. Today 100 (2005) 79.
[54] B.M. Weckhuysen, D.E. Keller, Catal. Today 78 (2003) 25.
[55] G. Kresse, J. Furthmüller, Phys. Rev. B 54 (1996) 11169.
[56] G. Kresse, J. Furthmüller, Comput. Mater. Sci. 6 (1996) 15.
[57] G. Kresse, D. Joubert, Phys. Rev. B 59 (1999) 1758.
[58] J.P. Perdew, Y. Wang, Phys. Rev. B 45 (1992) 13244.
[59] J.A. Dean, Lange's Handbook of Chemistry, McGraw-Hill Inc., New York, 1992.
[60] G.V. Samsonov, The Oxide Handbook, IFI/Plenum, New York, 1982.
[61] C.H. Bates, W.B. White, R. Roy, Science 137 (1962) 993.
[62] B. Meyer, D. Marx, Phys. Rev. B 67 (2003) 035403.
[63] G. Kresse, O. Dulub, U. Diebold, Phys. Rev. B 68 (2003) 245409.
[64] S. Chrétien, H. Metiu, J. Chem. Phys. 129 (2008) 0747705.
[65] H.Y. Kim, R.G.S. Pala, V. Shapovalov, H.M. Lee, H. Metiu, J. Phys. Chem. C 112 (2008) 12398.
[66] C. Doornkamp, V. Ponec, J. Mol. Catal. A 162 (2000) 19.
[67] R. Bader, Atoms in Molecules: A Quantum Theory, Clarendon, Oxford, 1994.
[68] G. Henkelman, A. Arnaldsson, H. Jonsson, Comput. Mater. Sci. 36 (2006) 354.
[69] L.F. Liao, C.F. Lien, D.L. Sieh, J.L. Lin, J. Phys. Chem. B 106 (2002) 11240.
[70] S. Wendt, R. Schaub, J. Matthiesen, E.K. Vestergaard, E. Wahlstrom, M.D. Rasmussen, P. Thostrup, L.M. Molina, E. Laegsgaard, I. Stensgaard, B. Hammer, F. Besenbacher, Surf. Sci. 598 (2005) 226.
[71] M.A. Henderson, W.S. Epling, C.L. Perkins, C.H.F. Peden, U. Diebold, J. Phys. Chem. B 103 (1999) 5328.
[72] W.S. Epling, C.H.F. Peden, M.A. Henderson, U. Diebold, Surf. Sci. 412–413 (1998) 333.